



Enhanced carrier confinement and radiative recombination in GaN-based lasers by tailoring first-barrier doping

JIANXUN LIU,^{1,2}  HAORAN QIE,^{1,3} QIAN SUN,^{1,2,3,*} MEIXIN FENG,^{1,2,3} JIN WANG,¹ XIUJIAN SUN,¹ XING SHENG,⁴  MASAO IKEDA,¹ AND HUI YANG^{1,3}

¹Key Laboratory of Nanodevices and Applications, Suzhou Institute of Nano-Tech and Nano-Bionics (SINANO), Chinese Academy of Sciences (CAS), Suzhou 215123, China

²Guangdong (Foshan) Branch, SINANO, CAS, Foshan 528200, China

³School of Nano Technology and Nano Bionics, University of Science and Technology of China, Hefei 230026, China

⁴Department of Electronic Engineering, Tsinghua University, Beijing 100084, China

*qsum2011@sinano.ac.cn

Abstract: Very limited 1-3 pairs of quantum-wells (QWs) are preferred for GaN-based laser diodes (LDs), which require more careful engineering of the carrier transport than LEDs. In this work, the first-barrier doping level of QWs is found to significantly affect the carrier confinement and distribution for GaN-based LDs. The first-barrier doping exceeding $2 \times 10^{18} \text{ cm}^{-3}$ will make the bottom QW return to the parasitic state, yielding unexpected photons absorption and even Auger recombination. The underlying physical mechanism is discussed in terms of the calculated energy-band diagram, carrier confinement, and distribution. And all the experimental findings are consistent with the physical model.

© 2020 Optical Society of America under the terms of the [OSA Open Access Publishing Agreement](#)

1. Introduction

Gallium nitride (GaN) based laser diodes (LDs) are drawing greater attention in solid-state lighting, display, sensor and visible light communications, owing to their unique blue-green spectral range, superior brightness, efficiency, and modulation bandwidth [1–4]. Compared with light-emitting diodes (LEDs) that typically have 5-10 pairs of quantum-wells (QWs) [5–6], very limited 1-3 pairs of QWs is preferred for GaN-based LDs [7–8]. The primary reason is that population inversion is required for lasing action where more QWs would call for higher carrier injection to activate every QW. The extra carrier injection before lasing not only leads to an enhancement of the Auger recombination (proportional to the cube of carrier concentration) [9], but also causes the carrier delocalization [10] and increases the carrier leakage [11], hence reducing the internal quantum efficiency, which is well known as the “efficiency droop” in LEDs [12]. A second reason for such few QWs configuration in GaN-based LDs is the largely non-uniform distribution of carriers and gain profile due to the asymmetric doping and carrier transport, which is observed as the *p*-side QWs contributing most of radiative recombination and light emission [13]. As a consequence, the *p*-side QWs are likely to reach population inversion first and produce the optical gain earlier. In contrast, the *n*-side QWs can absorb photons generated by other QWs, causing the local gain one order of magnitude lower than that of the *p*-side [14]. This non-uniform gain profile has been reported to result in a significant increase in the threshold current of GaN-based LDs [15,16].

Reducing the number of QWs partly alleviates the carrier non-uniformity, but the carrier leakage becomes more prevalent due to the insufficient thermalization or inefficient capture into the QW [17]. Moreover, because of the inherent polarization effect of *c*-plane QWs, the energy

band is tilted. This not only spatially separates the injected carriers and reduces the radiative recombination rate, but also decreases the effective barrier height thus degrading the carrier confinement [18]. Therefore, it is vitally important to enhance the carrier confinement for the GaN-based LDs, which however has rarely been studied so far.

Efforts have been paid to improve the electron confinement by various designs of electron-blocking layer (EBL) for electrons [19–22]. However, very little work has been done on the enhancement of hole confinement in GaN-based LDs, which has been proposed as one more leading factor that affects the LD performance [23,24]. By virtue of the ability to modify the built-in electric field and affect the carrier transport, barrier doping promises to improve both the electron and hole confinement for GaN-based LDs that have very limited 1-3 pairs of QWs. In fact, the barrier doping has been widely reported to significantly affect the photoluminescence (PL) and electroluminescence (EL) performance of GaN-based LEDs owing to superior band engineering, such as improving the PL intensity of InGaN/GaN MQWs by 33 times [25], a 37.5% enhancement in light-output power of one-QB-doped ($3 \times 10^{18} \text{ cm}^{-3}$) LEDs over all-QB-doped ones by Zhu *et al.* [26], a factor of 3.17 for the output power of all-QB-doped ($3 \times 10^{18} \text{ cm}^{-3}$) LEDs compared with the all-QB-undoped LEDs by Lu *et al.* [27], over 25% increase in the output power of InGaN/GaN LEDs upon carefully selecting the doping level and position by Tsai *et al.* [28], as well as a significant increase of luminous intensity from 25 to 36 mcd, and a decrease of the forward voltage from 4.5 to 3.5 V under the QB Si-doping of $3 \times 10^{17} \text{ cm}^{-3}$ for GaN-based LEDs [29]. However, a high Si-doping level in all the barriers will block the hole injection [30], and induce free-carrier absorption which increases the threshold current in the case of LDs [31]. Therefore, a fine tailoring of the barrier doping that provide a better understanding and a good balance between the carrier confinement and optical loss, is urgently needed for GaN-based LDs.

In this work, the first-barrier doping level of MQWs is found to significantly affect the carrier confinement and radiative recombination for GaN-based LDs by both simulations and experiments. The corresponding physical mechanism is discussed in terms of the calculated energy band diagram, carrier confinement, distribution, and recombination. And all the experimental findings are consistent with the physical model.

2. Experiments

Schematic diagram of the GaN-based laser and Si doping level of the first barrier used in the simulations are shown in Fig. 1. The LD structure is composed of a 2- μm -thick undoped GaN layer, an 1.3- μm -thick n-type GaN layer, an 1.2- μm -thick Si-doped n-Al_{0.075}Ga_{0.925}N optical cladding layers (n-CL), a 50-nm-thick undoped GaN waveguide layer, a 80-nm-thick undoped In_{0.01}Ga_{0.99}N lower waveguide layer (LWG), a 10-nm-thick GaN first barrier with various Si doping from 0 to $4 \times 10^{18} \text{ cm}^{-3}$, 3 pairs of undoped In_{0.12}Ga_{0.88}N (2.8 nm) / In_{0.01}Ga_{0.99}N (12 nm) MQWs, a 70-nm-thick undoped In_{0.01}Ga_{0.99}N upper waveguide layer (UWG), a 20-nm-thick undoped GaN waveguide layer, a 20-nm-thick Mg-doped p-Al_{0.2}Ga_{0.8}N EBL, a 600-nm-thick Mg-doped p-Al_{0.065}Ga_{0.935}N optical cladding layers (p-CL) and finally a 30-nm-thick Mg-doped p-GaN layer. The self-consistent Schrödinger-Poisson equations combined with polarization engineering theory was employed to calculate the band profile and carrier distribution of the LD structure, using the one-dimensional Schrödinger-Poisson solver containing the drift-diffusion and polarization model [32]. The conduction-to-valence-band offset ratio was set to be 0.67:0.33 [14,33]. Detailed material parameters used in this simulation can be found in the book edited by Joachim Piprek [34].

The test LD structure used to examine the carrier confinement was grown by metal-organic chemical vapor deposition on Si(111) substrates with an AlN/AlGa_{0.3}N buffer grown first followed by the layers shown in Fig. 1. The threading dislocation density (TDD) of the test LD epitaxial structures were confirmed by high resolution X-ray diffraction rocking curve of the GaN (0002)

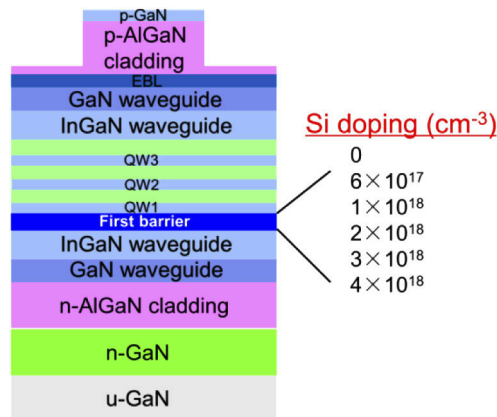


Fig. 1. Schematic diagram of the GaN-based laser structure with various Si doping of the first barrier from 0 to $4 \times 10^{18} \text{ cm}^{-3}$.

and $(10\bar{1}2)$ planes, all of which present a TDD of about $6 \times 10^8 \text{ cm}^{-2}$. The LD epitaxial wafers were then fabricated as ridge waveguide LDs and cleaved into discrete bars for testing. Detailed 3D schematics and pictures of the fabricated LDs can be found in our previous publications [2,8]. The on-bar EL measurements of the LDs were performed under a pulsed injection with a repetition rate of 10 kHz and a pulse width of 400 ns to minimize the self-heating effects.

3. Results and discussion

Figure 2(a) illustrates the conduction band diagrams near the active region with various Si doping of the first barrier at an equilibrium state. A clear potential gradient from the n -side to p -side QWs can be observed for the active region with no doping for the first barrier. This makes it energetically favorable for electrons to escape to the p -side. As the first-barrier doping increases, the height of the n -side conduction band rapidly decreases, and the potential gradient among QWs tends to disappear. As a result, an almost flat active region can be obtained as shown in Figs. 2(a)–2(b), which minimizes the driving force for electrons to overflow. Such variation is indeed the result of the field compensation between the p-n junction field shifted by first-barrier doping and the piezoelectric field in the MQWs, finally determining the alignment of internal field and active region. Similar confinement enhancement for hole injection can be found based on the valence band diagrams in Fig. 2(b). Therefore, the injection efficiency of both the electrons and holes are expected to be enhanced by controlling the first-barrier doping. This view is further confirmed by the dependence of QW depth on the first-barrier doping, as shown in Fig. 2(c). The average depth of the three QWs increases from 113.7 to 152.3 meV as the first-barrier doping increases from 0 to $4 \times 10^{18} \text{ cm}^{-3}$. The increased QW depth entails a larger effective volume that allows for much more carrier capture and hence better carrier confinement.

To study the carrier transport with respect to the first-barrier doping of the LD active region, further simulations were performed under a forward bias of 5 V. The cooling energy (Δn , Δp) corresponds to the kinetic energy drop of carrier thermalization through the emission of multiple longitudinal optical phonons before they reaching the first QW, as shown in Fig. 3(a). The overflow barrier ($\Delta n'$, $\Delta p'$) represents the barrier height for carriers escaping from the last QW, as shown in Fig. 3(b). The statistical results for carrier cooling energy and overflow barrier can be found in Figs. 3(c)–3(d). The cooling energy Δn for electrons (Fig. 3(c)) progressively increases with respect to the first-barrier doping, indicating an enhanced thermalization which particularly discourages the electron overflow under a high injection. The increased overflow barrier $\Delta n'$ also suggests better electron confinement as the first-barrier doping increases. However, compared

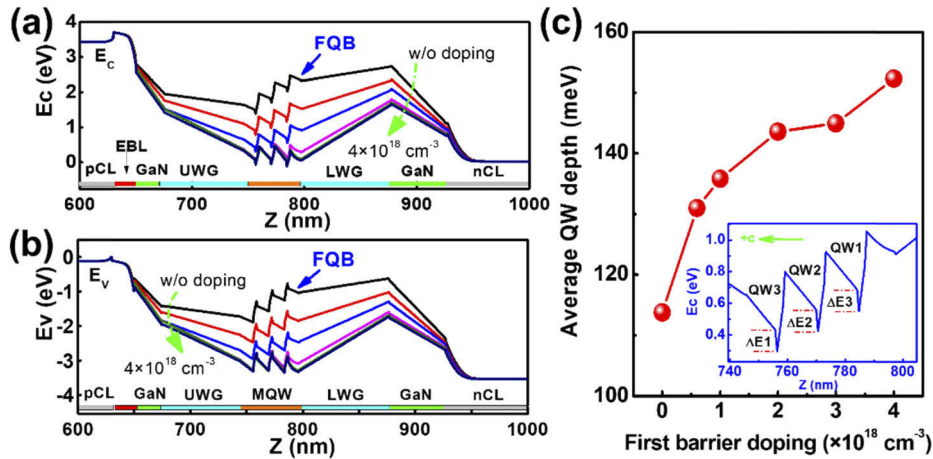


Fig. 2. (a) Conduction band and (b) valence band diagrams of the GaN-based LDs at an equilibrium state. (c) The average QW depth as a function of the first-barrier doping as extracted in the inset.

with electrons, both the cooling energy Δp and overflow barrier $\Delta p'$ for holes reach the maximum at the doping of $2 \times 10^{18} \text{ cm}^{-3}$. Further increasing the doping of the first barrier leads to significant degradation of the hole confinement, as shown in Fig. 3(d). Therefore, the optimum design of first-barrier doping requires a careful trade-off between the electron and hole confinement.

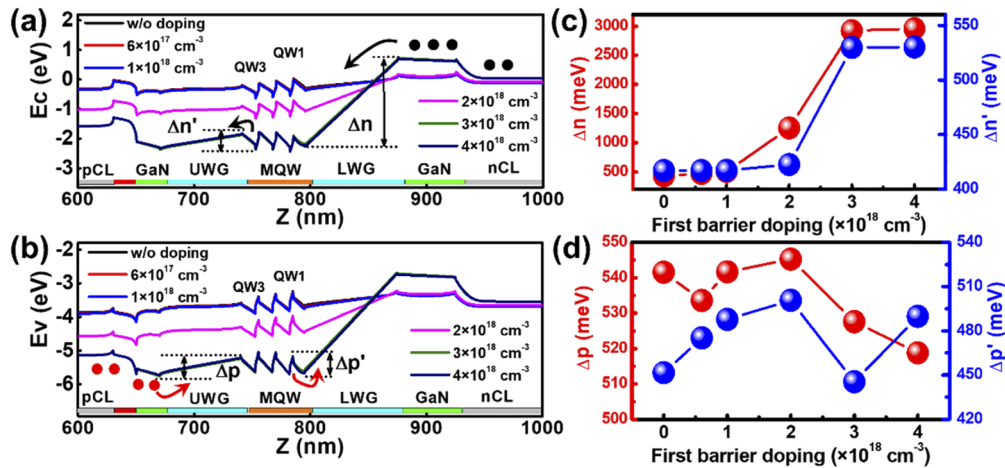


Fig. 3. (a) Conduction band and (b) valence band diagrams of the GaN-based LDs under a forward bias of 5 V. The cooling energy and overflow barrier for (c) electron (Δn and $\Delta n'$) and (d) hole (Δp and $\Delta p'$) as a function of the first-barrier doping.

Beyond the carrier confinements, the carrier distribution among MQWs is also critical in determining the total gain of the LD active region. The local carrier distribution profile of the LD structure is far from uniform when the first barrier is nominally un-doped, as illustrated in Fig. 4. The electron mainly concentrates in the p -side QW (QW3) while the hole largely locates in the n -side QW (QW1). This hole distribution is exactly opposite with the typically observed in GaN-based LEDs [35], which can be partially explained by the major potential gradient among QWs (as illustrated in Fig. 3). Due to the significantly asymmetric distribution of

the carriers, the holes in QW1 and the electrons in QW3 are favorable to leak out or recombine non-radiatively due to the radiative recombination saturation [36]. It is noteworthy that the asymmetric distribution of electrons and holes can be suppressed when the Si doping of the first barrier increases from 0 to $4 \times 10^{18} \text{ cm}^{-3}$. The maximum hole concentration is shifted from the *n*-side QW (QW1) to the middle one (QW2) as the first-barrier doping increases to $2 \times 10^{18} \text{ cm}^{-3}$, which can significantly reduce the hole leakage into the *n* side. However, when the first-barrier doping exceeds $2 \times 10^{18} \text{ cm}^{-3}$, the asymmetric distribution of carriers becomes prevalent again, with the hole concentration in QW1 getting lower while the electron concentration increasing. The former is in line with the degraded hole confinement at a heavy doping ($> 2 \times 10^{18} \text{ cm}^{-3}$) as depicted in Fig. 3(d), and the latter is attributed to the enhanced electron confinement as illustrated in Fig. 3(c). Such asymmetric distribution of carriers makes the QW1 return to the parasitic QW state, which not only yields Auger recombination, but also absorbs photons generated by the other two wells, thus reducing the optical gain and increasing the threshold current of GaN-based LD. Previous report by Piprek *et al.* [37] proposed using two QWs instead to improve the carrier distribution. Here the Si-doping control of the first barrier could be an alternative method to address this problem. Therefore, the optimum design of the first-barrier doping is believed to be $2 \times 10^{18} \text{ cm}^{-3}$ considering both the carrier confinement and distribution.

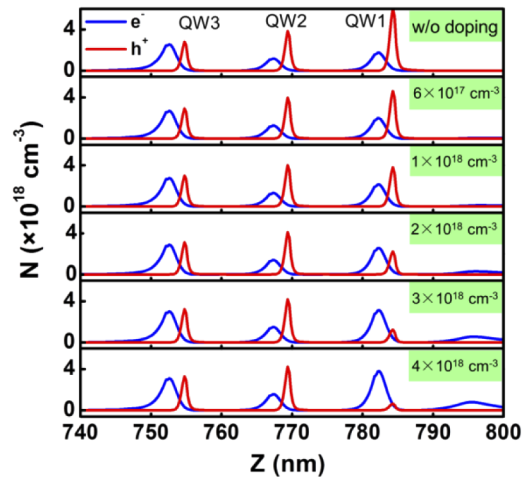


Fig. 4. The electron and hole concentration in the MQWs active region with various first-barrier doping under a forward bias of 5 V.

To validate the simulations above, three GaN-based LDs with various first-barrier doping of 0, 2×10^{18} and $3 \times 10^{18} \text{ cm}^{-3}$ were grown on Si substrates, and then fabricated as ridge waveguide LDs with a ridge width of $4 \mu\text{m}$ and a cavity length of $800 \mu\text{m}$ by conventional lithography and a lift-off technique. The cavities and mirror facets were formed by cleaving along the *m*-plane with no reflective coating on the facets. Figure 5(a) shows the typical lasing spectra of the three GaN-based LDs. The small variation in lasing wavelength is mainly caused by the unintentional fluctuation in growth temperature of the MQWs, rather than by the first-barrier doping. Figure 5(b) presents the power-current (P-I) curves and far-field patterns (FFP) of the GaN-based LDs. The super-linear P-I curves, elliptical FFP above threshold current, together with the narrow spectral linewidth, exactly demonstrate the lasing behavior. Figure 5(c) shows statistical distribution of the measured threshold currents for more than 60 devices. The threshold current of more than 70% of the devices is distributed around the average value, making it representative to compare the effects of first-barrier doping on band structure and carrier confinement. Due to the uncoated cavity facets, the threshold current density of all on-bar test LDs is larger than our

previous reports [2,8]. The open circles represent the average threshold current. It is clear that the average threshold current quickly drops from 435 (13.6 kA/cm²) to 280 mA (8.7 kA/cm²) with the first-barrier doping of 2×10^{18} cm⁻³, but further increases to 452 mA (14.1 kA/cm²) when the first-barrier doping reaches 3×10^{18} cm⁻³. This result correlates very well with the simulations above that the Si doping of 2×10^{18} cm⁻³ better balances the electron and hole confinement, and symmetric distribution. Also, the considerably increased threshold current at the doping of 3×10^{18} cm⁻³ or even higher doping for the first barrier may also be related to the degraded interface quality and increased band-tail absorption caused by Si heavy doping. Therefore, a Si doping of around 2×10^{18} cm⁻³ for the first barrier can be the optimum design for GaN-based LDs with three pairs of QWs. Simulations on the effects of QW number and QW wavelength are currently under intensive investigation, and the results with experimental validation will be published elsewhere.

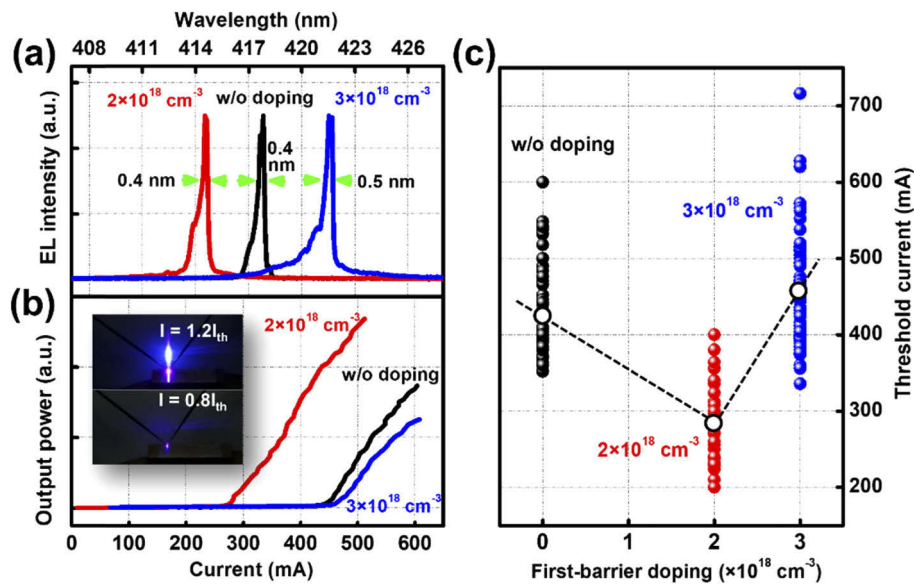


Fig. 5. (a) Typical lasing spectra and (b) P-I curves near the average threshold current for GaN-based lasers with various first-barrier doping. The inset shows the far-field patterns. (c) Statistical distribution of the threshold currents with the open circles representing the average value.

4. Conclusion

In summary, the effects of first-barrier doping on the carrier confinement and re-distribution in GaN-based LDs have been studied by both simulations and experiments. The electron confinement can be progressively enhanced with respect to the first-barrier doping, while the best hole confinement occurs at the doping of 2×10^{18} cm⁻³. Moreover, the first-barrier doping exceeding 2×10^{18} cm⁻³ was found to make the bottom quantum-well return to the parasitic absorbing state, yielding unexpected photons absorption and even Auger recombination, thus increasing the threshold current of GaN-based LDs. A Si doping of around 2×10^{18} cm⁻³ for the first barrier was finally suggested for GaN-based LDs with three pairs of QWs configuration, which can better enhance the carrier confinement and symmetrize the carrier distribution, hence improving the optical gain and reducing the threshold current of GaN-based LDs as confirmed experimentally as well.

Funding

Key-Area R&D Program of Guangdong Province (2019B010130001, 2019B090904002, 2019B090909004, 2019B090917005, 2020B010174004); National Natural Science Foundation of China (61534007, 61775230, 61804162, 61874131); Strategic Priority Research Program of CAS (XDB43000000, XDB43020200); Key Research Program of Frontier Sciences, CAS (QYZDB-SSW-JSC014, ZDBS-LY-JSC040); CAS Interdisciplinary Innovation Team; Natural Science Foundation of Jiangsu Province (BK20180253); Natural Science Foundation of Jiangxi Province (20181ACB20002); Suzhou Science and Technology Program (SYG201927); China Postdoctoral Science Foundation (2018M632408); Open Fund of the State Key Laboratory of Reliability and Intelligence of Electrical Equipment (EERIKF2018001).

Acknowledgments

The authors are grateful for the technical supports from Nano Fabrication Facility, Platform for Characterization & Test, and Nano-X of SINANO, CAS.

Disclosures

The authors declare no conflicts of interest.

References

1. J. Y. Tsao, M. H. Crawford, M. E. Coltrin, A. J. Fischer, D. D. Koleske, G. S. Subramania, G. T. Wang, J. J. Wierer, and R. F. Karlicek Jr, "Toward Smart and Ultra-efficient Solid-State Lighting," *Adv. Opt. Mater.* **2**(9), 809–836 (2014).
2. Y. Sun, K. Zhou, Q. Sun, J. Liu, M. Feng, Z. Li, Y. Zhou, L. Zhang, D. Li, S. Zhang, M. Ikeda, S. Liu, and H. Yang, "Room-temperature continuous-wave electrically injected InGa_N-based laser directly grown on Si," *Nat. Photonics* **10**(9), 595–599 (2016).
3. M. Khoury, H. Li, H. Zhang, B. Bonef, M. S. Wong, F. Wu, D. Cohen, P. De Mierry, P. Vennéguès, J. S. Speck, S. Nakamura, and S. P. DenBaars, "Demonstration of Electrically Injected Semipolar Laser Diodes Grown on Low-Cost and Scalable Sapphire Substrates," *ACS Appl. Mater. Interfaces* **11**(50), 47106–47111 (2019).
4. C. Shen, T. K. Ng, J. T. Leonard, A. Pourhashemi, H. M. Oubei, M. S. Alias, S. Nakamura, S. P. DenBaars, J. S. Speck, A. Y. Alyamani, M. M. Eldesouki, and B. S. Ooi, "High-Modulation-Efficiency, Integrated Waveguide Modulator-Laser Diode at 448 nm," *ACS Photonics* **3**(2), 262–268 (2016).
5. C. Jia, T. Yu, H. Lu, C. Zhong, Y. Sun, Y. Tong, and G. Zhang, "Performance improvement of GaN-based LEDs with step stage InGa_N/Ga_N strain relief layers in GaN-based blue LEDs," *Opt. Express* **21**(7), 8444–8449 (2013).
6. Y. Li, S. You, M. Zhu, L. Zhao, W. Hou, T. Detchprohm, Y. Taniguchi, N. Tamura, S. Tanaka, and C. Wetzel, "Defect-reduced green GaIn_N/Ga_N light-emitting diode on nanopatterned sapphire," *Appl. Phys. Lett.* **98**(15), 151102 (2011).
7. Y. Sun, K. Zhou, M. Feng, Z. Li, Y. Zhou, Q. Sun, J. Liu, L. Zhang, D. Li, and X. Sun, "Room-temperature continuous-wave electrically pumped InGa_N/Ga_N quantum well blue laser diode directly grown on Si," *Light: Sci. Appl.* **7**(1), 13 (2018).
8. J. Liu, J. Wang, X. Sun, Q. Sun, M. Feng, X. Ge, J. Ning, R. Zhou, Y. Zhou, H. Gao, M. Ikeda, and H. Yang, "Performance improvement of InGa_N-based laser grown on Si by suppressing point defects," *Opt. Express* **27**(18), 25943–25952 (2019).
9. M. Zhang, P. Bhattacharya, J. Singh, and J. Hinckley, "Direct measurement of auger recombination in In_{0.1}Ga_{0.9}N/GaN quantum wells and its impact on the efficiency of In_{0.1}Ga_{0.9}N/GaN multiple quantum well light emitting diodes," *Appl. Phys. Lett.* **95**(20), 201108 (2009).
10. T. J. Badcock, S. Hammersley, D. Watson-Parris, P. Dawson, M. J. Godfrey, M. J. Kappers, C. McAleese, R. A. Oliver, and C. J. Humphreys, "Carrier Density Dependent Localization and Consequences for Efficiency Droop in InGa_N/Ga_N Quantum Well Structures," *Jpn. J. Appl. Phys.* **52**(8S), 08JK10 (2013).
11. Q. Dai, Q. Shan, J. Cho, E. F. Schubert, M. H. Crawford, D. D. Koleske, M.-H. Kim, and Y. Park, "On the symmetry of efficiency-versus-carrier-concentration curves in GaIn_N/Ga_N light-emitting diodes and relation to droop-causing mechanisms," *Appl. Phys. Lett.* **98**(3), 033506 (2011).
12. M.-H. Kim, M. F. Schubert, Q. Dai, J. K. Kim, E. F. Schubert, J. Piprek, and Y. Park, "Origin of efficiency droop in GaN-based light-emitting diodes," *Appl. Phys. Lett.* **91**(18), 183507 (2007).
13. A. David, M. J. Grundmann, J. F. Kaeding, N. F. Gardner, T. G. Mihopoulos, and M. R. Krames, "Carrier distribution in (0001) InGa_N/Ga_N multiple quantum well light-emitting diodes," *Appl. Phys. Lett.* **92**(5), 053502 (2008).

14. W. Yang, D. Li, N. Liu, Z. Chen, L. Wang, L. Liu, L. Li, C. Wan, W. Chen, X. Hu, and W. Du, "Improvement of hole injection and electron overflow by a tapered AlGaIn electron blocking layer in InGaIn-based blue laser diodes," *Appl. Phys. Lett.* **100**(3), 031105 (2012).
15. D. S. Sizov, R. Bhat, A. Zakharian, J. Napierala, K. Song, D. Allen, and C.-e. Zah, "Impact of Carrier Transport on Aquamarine-Green Laser Performance," *Appl. Phys. Express* **3**(12), 122101 (2010).
16. J. Piprek, P. Abraham, and J. E. Bowers, "Cavity length effects on internal loss and quantum efficiency of multi-quantum-well lasers," *IEEE J. Sel. Top. Quantum Electron.* **5**(3), 643–647 (1999).
17. M. Grupen and K. Hess, "Simulation of carrier transport and nonlinearities in quantum-well laser diodes," *IEEE J. Quantum Electron.* **34**(1), 120–140 (1998).
18. Y.-K. Kuo, J.-Y. Chang, M.-C. Tsai, and S.-H. Yen, "Advantages of blue InGaIn multiple-quantum well light-emitting diodes with InGaIn barriers," *Appl. Phys. Lett.* **95**(1), 011116 (2009).
19. S.-N. Lee, S. Y. Cho, H. Y. Ryu, J. K. Son, H. S. Paek, T. Sakong, T. Jang, K. K. Choi, K. H. Ha, M. H. Yang, O. H. Nam, Y. Park, and E. Yoon, "High-power GaIn-based blue-violet laser diodes with AlGaIn/GaIn multi-quantum barriers," *Appl. Phys. Lett.* **88**(11), 111101 (2006).
20. L. C. Le, D. G. Zhao, D. S. Jiang, P. Chen, Z. S. Liu, J. Yang, X. G. He, X. J. Li, J. P. Liu, J. J. Zhu, S. M. Zhang, and H. Yang, "Suppression of electron leakage by inserting a thin undoped InGaIn layer prior to electron blocking layer in InGaIn-based blue-violet laser diodes," *Opt. Express* **22**(10), 11392–11398 (2014).
21. Y. Zhang, T.-T. Kao, J. Liu, Z. Lochner, S.-S. Kim, J.-H. Ryou, R. D. Dupuis, and S.-C. Shen, "Effects of a step-graded Al_xGa_{1-x}In electron blocking layer in InGaIn-based laser diodes," *J. Appl. Phys.* **109**(8), 083115 (2011).
22. D. H. Hsieh, A. J. Tzou, T. S. Kao, F. I. Lai, D. W. Lin, B. C. Lin, T. C. Lu, W. C. Lai, C. H. Chen, and H. C. Kuo, "Improved carrier injection in GaIn-based VCSEL via AlGaIn/GaIn multiple quantum barrier electron blocking layer," *Opt. Express* **23**(21), 27145–27151 (2015).
23. T. Hager, M. Binder, G. Bröderl, C. Eichler, A. Avramescu, T. Wurm, A. Gomez-Iglesias, B. Stojetz, S. Tautz, B. Galler, S. Gerhard, R. Zeisel, and U. Strauss, "Carrier transport in green AlInGaIn based structures on *c*-plane substrates," *Appl. Phys. Lett.* **102**(23), 231102 (2013).
24. Y. Cheng, J. Liu, A. Tian, F. Zhang, M. Feng, W. Hu, S. Zhang, M. Ikeda, D. Li, L. Zhang, and H. Yang, "Hole transport in *c*-plane InGaIn-based green laser diodes," *Appl. Phys. Lett.* **109**(9), 092104 (2016).
25. M.-K. Kwon, I.-K. Park, S.-H. Beak, J.-Y. Kim, and S.-J. Park, "Improvement of photoluminescence by Si delta-doping in GaIn barrier layer of GaIn/In_xGa_{1-x}In multi-quantum wells," *Phys. Status Solidi A* **202**(5), 859–862 (2005).
26. D. Zhu, A. N. Noemaun, M. F. Schubert, J. Cho, E. F. Schubert, M. H. Crawford, and D. D. Koleske, "Enhanced electron capture and symmetrized carrier distribution in GaInN light-emitting diodes having tailored barrier doping," *Appl. Phys. Lett.* **96**(12), 121110 (2010).
27. Y.-H. Lu, Y.-K. Fu, S.-J. Huang, Y.-K. Su, Y.-C. Chen, R. Xuan, and M. H. Pilkuhn, "Suppression of Nonradiation Recombination by Selected Si Doping in AlGaIn Barriers for Ultraviolet Light-Emitting Diodes," *Jpn. J. Appl. Phys.* **52**(8S), 08JL15 (2013).
28. P.-C. Tsai, Y.-K. Su, W.-R. Chen, and C.-Y. Huang, "Enhanced Luminescence Efficiency of InGaIn/GaIn Multiple Quantum Wells by a Strain Relief Layer and Proper Si Doping," *Jpn. J. Appl. Phys.* **49**(4), 04DG07 (2010).
29. L. W. Wu, S. J. Chang, T. C. Wen, Y. K. Su, J. F. Chen, W. C. Lai, C. H. Kuo, C. H. Chen, and J. K. Sheu, "Influence of Si-doping on the characteristics of InGaIn-GaIn multiple quantum-well blue light emitting diodes," *IEEE J. Quantum Electron.* **38**(5), 446–450 (2002).
30. Z.-H. Zhang, W. Liu, Z. Ju, S. T. Tan, Y. Ji, Z. Kyaw, X. Zhang, L. Wang, X. W. Sun, and H. V. Demir, "Self-screening of the quantum confined Stark effect by the polarization induced bulk charges in the quantum barriers," *Appl. Phys. Lett.* **104**(24), 243501 (2014).
31. J. Chen, C. Lee, T. Ko, Y. Chang, T. Lu, H. Kuo, Y. Kuo, and S. Wang, "Effects of Built-In Polarization and Carrier Overflow on InGaIn Quantum-Well Lasers With Electronic Blocking Layers," *J. Lightwave Technol.* **26**(3), 329–337 (2008).
32. C.-K. Li, M. Piccardo, L.-S. Lu, S. Mayboroda, L. Martinelli, J. Peretti, J. S. Speck, C. Weisbuch, M. Filoche, and Y.-R. Wu, "Localization landscape theory of disorder in semiconductors. III. Application to carrier transport and recombination in light emitting diodes," *Phys. Rev. B* **95**(14), 144206 (2017).
33. J. Park, J. Lee, and S. Park, "Photoluminescence dependence of InGaIn/GaIn QW on embedded AlGaIn δ -layer," *Opt. Express* **15**(10), 6096–6101 (2007).
34. J. Piprek, *Nitride semiconductor devices: principles and simulation* (Wiley Online Library, 2007), Vol. 590.
35. J. P. Liu, J.-H. Ryou, R. D. Dupuis, J. Han, G. D. Shen, and H. B. Wang, "Barrier effect on hole transport and carrier distribution in InGaIn/GaIn multiple quantum well visible light-emitting diodes," *Appl. Phys. Lett.* **93**(2), 021102 (2008).
36. D.-S. Shin, D.-P. Han, J.-Y. Oh, and J.-I. Shim, "Study of droop phenomena in InGaIn-based blue and green light-emitting diodes by temperature-dependent electroluminescence," *Appl. Phys. Lett.* **100**(15), 153506 (2012).
37. J. Piprek, R. Sink, M. Hansen, J. Bowers, and S. DenBaars, "Simulation and optimization of 420-nm InGaIn/GaIn laser diodes," *Physics and Simulation of Optoelectronic Devices VIII. Symposium on Integrated Optoelectronics* 3944, 28–39 (2000).